

# Magnetic field effects on two-leg Heisenberg antiferromagnetic ladders: Thermodynamic properties

Xiaoqun Wang<sup>1</sup> and Lu Yu<sup>2,3</sup>

<sup>1</sup>*Institut Romand de Recherche Numerique en Physique Des Materiaux, PPH-333, EPFL, CH-1015 Lausanne, Switzerland*

<sup>2</sup>*International Center for Theoretical Physics, P. O. Box 586, 34100 Trieste, Italy*

<sup>3</sup>*Institute of Theoretical Physics, P. O. Box 2735, Beijing 100080, P.R. China*

Using the recently developed transfer-matrix renormalization group method, we establish a quantitative magnetic phase diagram of two-leg antiferromagnetic ladders. It contains disordered spin liquid, Luttinger liquid, spin-polarized phases and a classical regime. The boundaries between these regimes are determined by identifying the critical behavior of magnetization. Our findings in the low temperature regime clearly show that the divergence of the NMR relaxation rate observed on  $\text{Cu}_2(\text{C}_5\text{H}_{12}\text{N}_2)_2\text{Cl}_4$  can be well explained by the intrinsic properties of quasi-one-dimensional spin-gapped systems. The magnetic field effects on the specific heat are also explored in detail.

PACS numbers: 75.10.Jm, 75.40.Cx, 75.40.Mg

In the past several years, spin ladders have been at the focus of intensive research towards understanding the spin-1/2 Heisenberg antiferromagnets in one and two dimensions [1–5]. Experimentally, several classes of materials like  $\text{SrCu}_2\text{O}_3$ ,  $\text{La}_6\text{Ca}_8\text{Cu}_{24}\text{O}_{41}$  and  $\text{Cu}_2(\text{C}_5\text{H}_{12}\text{N}_2)_2\text{Cl}_4$  ( $\text{CuHpCl}$ ) have been found whose properties can be well described by the two-leg Heisenberg antiferromagnetic ladder (THAFL) model [6–8]. For inorganic oxides, the spin gap  $\Delta$  was found to be about  $500K$  [9]. Therefore, only the low-energy spectra can be feasibly explored by experimental measurements of spin susceptibility, NMR relaxation and neutron scattering [6,7,10]. On the other hand, the organo-metallic compound  $\text{CuHpCl}$  involves a very small spin gap  $\Delta \approx 11K$  [11] which allows a full investigation of the spectrum by applying a magnetic field (MF). Recently Chaboussant *et al.* have shown that the NMR rate exhibits significantly different behavior for different ranges of MF in the low temperature limit. On this basis these authors proposed a magnetic phase diagram [11,12]. Previously, some MF effects on THAFL were discussed by using bosonization and non-linear  $\sigma$ -model approaches [13–15]. In this paper, we provide the first calculations of the phase diagram using the newly developed transfer-matrix renormalization group (TMRG) technique [16]. Our findings allow to interpret the observed divergence of the NMR rate [11] as due to the MF effects on THAFL *i.e.*, quasi-1D rather than the 3D field-induced ordering when  $H \geq \Delta$ .

The Hamiltonian for the THAFL in our studies reads:

$$\mathcal{H} = \sum_{i=1} [J_{\parallel}(\mathbf{S}_{1,i} \cdot \mathbf{S}_{1,i+1} + \mathbf{S}_{2,i} \cdot \mathbf{S}_{2,i+1}) + J_{\perp} \mathbf{S}_{1,i} \cdot \mathbf{S}_{2,i} - H(S_{1,i}^z + S_{2,i}^z)], \quad H > 0 \quad (1)$$

where  $\mathbf{S}_{n,i}$  denotes a  $S=1/2$  spin operator at the  $i$ -th site of the  $n$ -th chain.  $J_{\parallel, \perp}$  are the intra- and inter-chain couplings, respectively. In the following, we set  $J_{\parallel}=1$ . Although magnetic phase diagram should be independent of the ratio  $J_{\perp}/J_{\parallel}$ , we have used  $J_{\perp}/J_{\parallel}=5.28$  to confront the experimental findings on  $\text{CuHpCl}$ .

The TMRG technique we adopt here is implemented in the thermodynamic limit and can be used to evaluate very accurately the thermodynamic quantities [16,17] as well as imaginary time auto-correlation functions [18,19] at very low- $T$  for quasi-1D systems. Technical aspects of this method can be found in Ref. [17]. In our calculations, the number of kept optimal states  $m=200$ , while the width of the imaginary time slice  $\epsilon=0.05$  are used in most cases. We have also used different  $m$  and  $\epsilon$  to verify the accuracy of calculations. The physical quantities presented below are usually calculated down to  $T \leq 0.02$ . The lowest temperature reached is  $T=0.005$ . The relative errors, being different for different quantities, are usually much less and at most about one percent for derivative quantities at very low temperatures.

We first determine the spin gap by fitting the spin susceptibility  $\chi$ , using the asymptotic formula proposed in [20]:  $\chi=Ae^{-\Delta/T}/\sqrt{T}$ ,  $T \rightarrow 0$ , based on the quadratic dispersion for the single magnon branch. Fitting numerical results  $\chi$  in the range  $T \in [0.168, 1]$  [21], we obtain  $\Delta=4.385$  which is very close to the value  $\Delta=4.382$  obtained using the  $T=0$  DMRG method ( $m=250$  states were kept and the extrapolation to infinite size was made).

Our main results are summarized in the quantitative magnetic phase diagram scaled by  $\Delta$ , shown in Fig. 1. The phase boundaries (or more precisely the crossover lines when  $T \neq 0$ ) are determined numerically on the basis of different MF dependence of the magnetization. At  $T=0$ : 1) as  $H < H_{C_1} = \Delta$ , the band edge state of the continuum spectrum has  $S_{total}^z = 1$ , with an effective gap  $\Delta_{eff}^{down} = H_{C_1} - H$ . The ground states are considered to be a kind of disordered spin liquids and thermodynamic quantities decrease exponentially at low  $T$ ; 2) As  $H_{C_1} \leq H \leq H_{C_2}$ , the gap vanishes and we find a range of linear in  $T$  dependence for the specific heat and finite values for the susceptibility, which is characteristic for the Luttinger liquid (LL); 3) The ground states become macroscopically polarized when  $H > H_{C_2}$  (a polarized

phase). There the thermodynamic quantities again behave exponentially with  $\Delta_{eff}^{up} = H - H_{C_2}$  at low  $T$ . The  $H$ -dependence of the gap is consistent with earlier numerical and analytical studies, [13–15] as well as with experimental findings [12]. Our new results mainly concern how these states would evolve and how the thermodynamic quantities change (see below) upon the increase of temperature. The LL regime shrinks gradually and disappears at  $T = T_0$ , while the other phases continue to exist until  $T = T_C$ . One finds a classical regime for  $T > T_C$ .

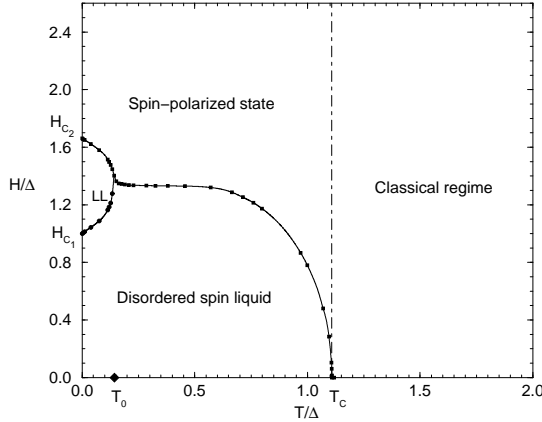


FIG. 1. Magnetic phase diagram in  $H - T$  plane

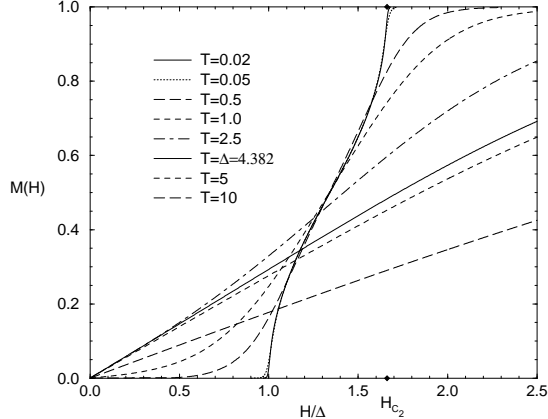


FIG. 2. Magnetization versus  $H$  for different  $T$

We use the critical behavior of the magnetization to identify various regimes in the  $H - T$  plane. In Fig. 2, we show the magnetization curves for different values of  $T \in [0.02, 10]$ . For quasi-1D spin-gapped systems, it is well-known that at  $T = 0$ ,  $M = 0$  for  $H \leq H_{C_1} = \Delta$ ;  $M = 1$  (in units of  $S$ ) for  $H \geq H_{C_2} = J_{\perp} + 2J_{\parallel}$  [8] and  $0 < M < 1$  for  $H \in (H_{C_1}, H_{C_2})$ . When  $T \neq 0$ ,  $M$  is nonzero for any  $H$ . However, the critical behavior of the magnetization for  $T = 0$  in the vicinity of  $H_{C_1}$  and  $H_{C_2}$  can only be seen at very low temperatures, and it is severely washed out for higher temperatures. The behavior of  $M(H)$  is elucidated in Fig. 3. Consider first

the  $T=0$  case in (a). We have calculated  $M(T=0)$  at  $H = 7.275, 7.25, 7.125, 700$  and  $4.4, 4.5, 4.625, 4.75$  for the upper and lower critical points, respectively. The calculations for  $M(T)$  were done with  $m=256$  down to  $T \approx 0.005$  (necessarily) for extrapolation to  $T=0$  limit. Then fitting  $M(T=0)$  at these  $H$  gives the following asymptotic form:

$$M(H) = \begin{cases} 0.380\sqrt{H - H_{C_1}} & \text{for } H = H_{C_1}^+ \\ 1 - 0.431\sqrt{H_{C_2} - H} & \text{for } H = H_{C_2}^- \end{cases} \quad (2)$$

consistent with the earlier studies [22,14,23]. Independently, we obtain  $H_{C_1} = 4.3823$  which is even more accurate than the value obtained from fitting  $\chi(T)$ .

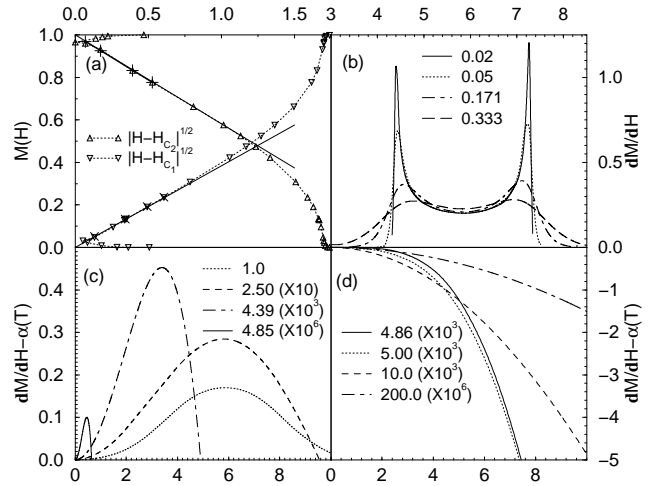


FIG. 3. Critical behavior of  $M(H)$ : (a) The asymptotic behavior of Eq. (2) denoted by solid lines.  $\times(+)$ :  $M(T=0)$  at  $H=H_{C_1}^+$  ( $H_{C_2}^-$ ),  $M(T=0.02)$  vs.  $\sqrt{|H - H_{C_{1,2}}|}$  (see legends) is shown for comparison only. (b)  $dM/dH$  vs  $H$  for  $T \leq T_0$  as indicated by legends; (c) For  $T_0 < T \leq T_C$ ; (d) For  $T > T_C$ . In (c) and (d), we subtract from the derivative a constant  $\alpha(T)$  and then amplify it as indicated in the parentheses.

When  $T > 0$ , depending on the behavior of  $dM/dH$ , there are three different cases: 1)  $dM/dH$  has a two-peak structure shown in Fig. 3(b) for  $T < T_0 = 0.59^{+0.04}$  (positive(negative) numbers in super(sub)-scripts are bounds of errors [21]), similar to the  $T=0$  case. 2) It has a single peak structure at  $H \neq 0$  in Fig. 3(c) for  $T_0 \leq T < T_C = 4.86_{-0.05}$ . 3) It reaches a maximum exactly at  $H = 0$  for  $T \geq T_C$  in Fig. 3(d). Suppose  $\gamma$  is the coefficient of the cubic term in the low- $H$  expansion of magnetization,  $T_C$  is given by  $\gamma(T_C) = 0$ . Then the boundaries, denoted by dots in Fig. 1, between the LL, the spin-polarized phase and the disordered spin liquid are given by those values of  $H$  and  $T$ , at which  $dM/dH$  is maximized.

We now elaborate more on the temperature dependence of  $M(T)$  for various given  $H$  as shown in Fig. 4. Consider a cooling process. For  $T > T_C \approx \Delta$ ,  $M$  monotonically but slowly increases for all  $H$ , whereas it can change non-monotonically depending upon the values of  $H$  for  $T < T_C$ . When  $H > H_{C_2}$ ,  $M$  continues to increase

and saturates exponentially with  $\Delta_{eff}^{up}$ . However, when  $H < H_{C_1}$ ,  $M$  first goes up, then down and finally decays to zero exponentially with  $\Delta_{eff}^{down}$ . When  $H_{C_1} < H < H_{C_2}$ , there is always a peak at  $T \neq 0$ . This peak is close to the boundary between the polarized phase and LL for  $H \geq H_m \approx 6$  [21], while separating the former from the disordered spin liquid phase elsewhere. There is also a minimum for LL. The positions of minima are at  $T = 0$  for  $H \geq H_m$ , otherwise they are close to the boundary of the LL regime.

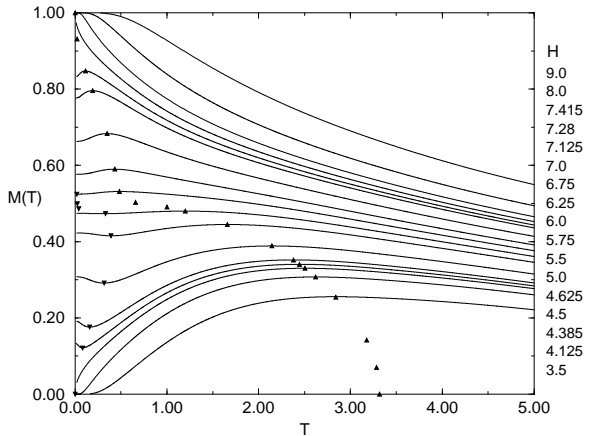


FIG. 4. Magnetization *vs.* temperature: Legends indicate  $H$  for the curves from top to bottom. The up (down)-triangles denote maxima (minima) at different  $H$ . Extra points added between curves are for maxima at  $H=7.25, 5.875, 5.812, 2.0, 1.0, 0, 0.005$  and minima at  $5.875, 5.812$ .

To interpret the above interesting feature, we recall that  $S_{total}^z$  is still a good quantum number for the Hamiltonian (1) and thus different energy bands are shifted by  $-S_{total}^z H$ . Moreover, the saturation for  $H > H_{C_2}$  and the decay for  $H < H_{C_1}$ , respectively, reflect two kinds of low-lying spectra: the fully polarized ground state and dominantly polarized low-lying excitations; the non-magnetic ground state and weakly polarized low-lying excitations. When  $H$  decreases from  $H_{C_2}$ , a peak appears instead of saturation, because the ground state is still a dominantly polarized state but no longer a fully polarized state (FPS). Then the FPS should be related to the position of the main peak at each  $H$  (the low-lying excitations within the range  $T_{peak}$  are “more” polarized states than the ground state for  $H > H_m$ ). The sharpness of the peak depends essentially on the density of states and the corresponding  $S_{total}^z$  near FPS in the spectrum. Those states near FPS are dominantly polarized with  $S_{total}^z > 0$  for  $H > H_m$  [21], but can be weakly polarized states or have  $S_{total}^z \leq 0$  when  $H < H_m$ . On the other hand, the minimum  $T \neq 0$  originates from low-lying states in  $S_{tot}^z = 0$  subspace. Those states intersect with FPS at  $H = H_m$ . Notably,  $H_m$  also corresponds to an extrapolation of the boundary between the two gapped phases in the phase diagram (Fig.1). It is also curious to note that in Fig.

4, the curves are roughly symmetric w.r.t.  $M = 0.5$ , if we focus on the low temperature part. This reflects the particle-hole symmetry of the problem in the fermion representation [14,12],

We now turn to the specific heat which, similar to  $M(T)$ , shows different behavior depending on  $H$ . When  $H < H_{C_1}$  in Fig. 5(a),  $C_v$  has a single peak structure as expected. The MF reduces  $\Delta_{eff}^{down}$ , and changes dramatically the line shape near  $T = 0.5$ , as  $H \rightarrow H_{C_1}^-$ . This is a signature of approaching the quantum critical point [25]. When  $H_{C_1} < H < H_{C_2}$  in Fig. 5(b) and (c), a second peak at low  $T$  is developed exhibiting the LL behavior. Linear- $T$  dependence is shown in the insets of (b) and (c). Moreover, at  $H = H_{C_1}^+$ , the cusp still remains and at  $H = H_{C_2}^-$  a shoulder emerges. When  $H \geq H_{C_2}$  in Fig. 5(d), the shoulder can still be seen for  $H = H_{C_2}^+$ , although the second peak vanishes. At low- $T$ ,  $C_v$  decreases exponentially with  $\Delta_{eff}^{up}$ . It is worth to notice that the cusps and shoulders appear outside the LL regime but near its boundary. For those  $H$  at which a larger second peak shows up, the local minima are also located outside the LL regime, but nearby.

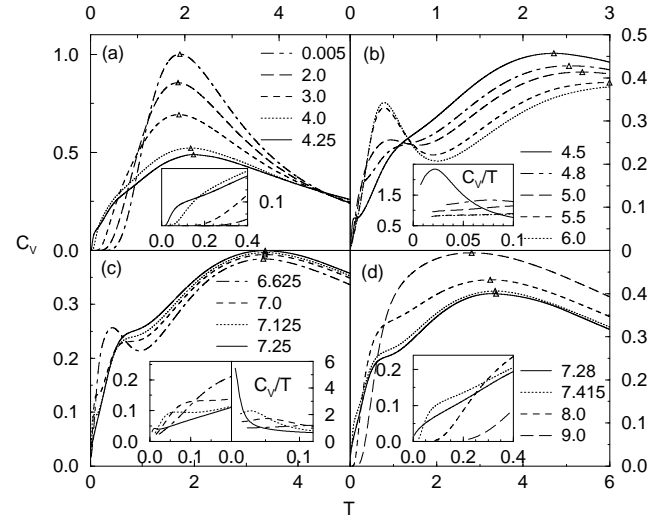


FIG. 5. Specific heat for various  $H$ : For  $H < H_{C_1}$  in (a);  $H_{C_1} < H < H_{C_2}$  in (b) and (c);  $H \geq H_{C_2}$  in (d). Insets: Low-T behavior in (a), the left one of (c) and (d);  $C_v/T$  in (b) and the right one of (c). Triangles denote maximum  $C_v$ .

It is also instructive to see the MF effects on the maximum specific heat  $C_v^{max}$  and corresponding temperature  $T_{max}$ . As seen in Fig. 6, when  $H$  is applied,  $C_v^{max}$  first declines as a gradual response to the splitting. At  $H = H_m$ , because of the crossing of two kinds of energy states discussed above,  $C_v^{max}$  arrives at a minimum. Moreover, we surprisingly found that the curvature of  $T_{max}$  changes its sign at  $H_{C_1}$ , while it reaches a maximum at  $H = H_{C_2}$ . These interesting features imply an intrinsic aspect of the MF effects as reflected consistently by the magnetization and the specific heat.

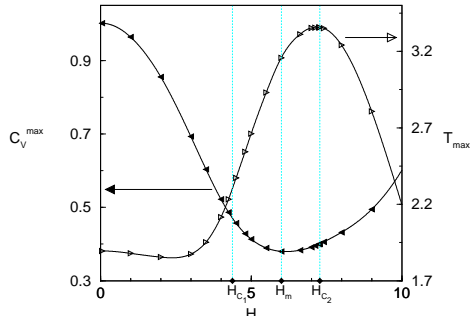


FIG. 6. The maximum specific heat  $C_v^{max}$  (to the left) and the corresponding temperature  $T_{max}$  (to the right) *versus*  $H$ .

Now we discuss the bearings of our numerical results on experimental findings [11,24] of a diverging NMR relaxation rate and peculiar specific heat behavior. Recently, Chaboussant *et al.* found that the NMR rate unusually increases for  $H_{C_1} \leq H \leq H_{C_2}$  when  $T$  decreases [11]. These authors attributed this anomalous increase to quasi-1D behavior. Our results show that it is indeed an intrinsic MF effect on the spin ladders. In fact, the increasing of the NMR rate starts already outside the LL regime which is bounded by  $T \approx 1.6K$ . This should share the same physical reason as the occurrence of the cusps and shoulders for  $C_v$  outside the LL regime. On the other hand, Hammar *et al.* [24] have measured  $C_v$  up to  $H = 9T$ , which is about  $(5.10 \pm 0.17)J_{\parallel}$ , taking into account the difference between the experimental and numerical results for the gap due to other interactions [13,12]. As seen in Fig. 3 of Ref. [24], the global feature is consistent with our results in Fig. 5(a) and (b), *e.g.* the shift of  $C_v^{max}$  and  $T_{max}$  as well as the abrupt change for  $H=6.6T$ . When  $H=9T$ , the 3D effect shows up for  $T \lesssim 0.32J_{\parallel}$  ( $0.81K$ ), which is about half of the width of the LL regime, and is a little below the second peak  $T'_{max} \approx 0.36J_{\parallel}$ , according to our results at  $H=5 \sim 5.5$  in Fig. 5(b). This means the observed behavior of  $C_v$  for  $T > 0.32J_{\parallel}$  can be explained within the THAFL, without resorting to 3D ordering. However, the second peak of the THAFL is too close to the 3D ordering temperature at  $H \sim 9T$ , so it is difficult to distinguish them. This was also why the unusual behavior of the NMR rate cannot be explained yet by the  $C_v$  measurements [11]. Therefore we would call for more detailed measurements to examine the second peak and shoulders with higher MFs for CuHgCl.

Finally, we note that our numerical results do not show clear signatures for the phase boundary of quantum critical regime, outlined in [11,12]. In addition, the classical regime is defined only by the weak temperature dependence of the thermodynamic quantities. However, we found  $T_C = 1.109 - 0.011\Delta$  instead of the usual expectation of  $T_C = \Delta$ .

In conclusion, we have established the magnetic phase diagram for the two-leg ladders. We emphasize that most of the striking MF effects show up for the LL regime,

which explains the divergence of the NMR rate observed in experiments. Moreover, this magnetic phase diagram is generically valid for other purely spin-gapped systems as well and the results on  $M(T)$  should also shed some light on other quasi-one dimensional fermion systems which involve either a charge gap or a band gap, but not a spin gap.

We are grateful to D. Loss, T.K. Ng, and B. Normand for fruitful discussions and to G. Chaboussant for helpful correspondence.

---

- [1] E. Dagotto and T.M. Rice, *Science*, **271**, 618(1996).
- [2] E. Dagotto, et al *Phys. Rev. B* **45**, 5744(1992).
- [3] T.M. Rice, S. Gopalan and M. Sigrist, *Europhys. Lett.* **23**, 445(1993); M. Sigrist, T.M. Rice and F.C. Zhang, *Phys. Rev. B* **49**, 12058(1994).
- [4] T. Barnes and J. Riera, *Phys. Rev. B* **50**, 6817 (1994).
- [5] X. Wang, [cond-mat/9803229](#).
- [6] M. Azuma, Z. Hiroi and M. Takano, *Phys. Rev. Lett.* **73**, 3463(1994).
- [7] T. Imai K.R. Thurber, K.M. Shen, A.W. Hunt and F.C. Chou, *Phys. Rev. Lett.* **81** 220 (1998).
- [8] G. Chaboussant, P.A. Crowell, L.P. Lévy, O. Piovesana, A. Madouri, and D. Mailly, *Phys. Rev. B* **55**, (1997) 3046.
- [9] D.C. Johnston, *Phys. Rev. B* **54**, 13009 (1996).
- [10] R. Eccleston, M. Uehara, J. Akimitsu, H. Eisaki, N. Motoyama and S. Uchida, [cond-mat/9711053](#)
- [11] G. Chaboussant, Y. Fagot-Revurat, M.-H. Julien, M.E. Hanson, C. Berthier, M. Horvatié, L.P. Lévy and O. Piovesana, *Phys. Rev. Lett.* **80** 2713 (1998).
- [12] G. Chaboussant *et al.*, [cond-mat/9811068](#).
- [13] C. Hawryard, D. Poilblanc and L.P. Lévy, *Phys. Rev.* **54**, (1996) 12649.
- [14] R. Chitra and T. Giamarchi, *Phys. Rev. B* **55**, 5816 (1997).
- [15] B. Norman, J. Kyriakidis, D. Loss, [cond-mat/9902104](#).
- [16] X. Wang and T. Xiang, *Phys. Rev. B* **56**, 56 (1997).
- [17] T. Xiang and X. Wang, *Lecture Notes in Physics: Density Matrix Renormalization*, Eds. I. Peschel, X. Wang, M. Kaulke and K. Hallberg (Springer, 1999).
- [18] T. Mutou, N. Shibata and K. Ueda, *Phys. Rev. Lett.* **81**, 4939 (1998).
- [19] F. Naef, X. Wang, X. Zotos and W. von der Linden, to appear in *Phys. Rev. B* on July 1, (1999).
- [20] M. Troyer, H. Tsunetsugu and D. Würtz, *Phys. Rev. B* **50**, 13515 (1994).
- [21] The detail will be discussed elsewhere.
- [22] G. I. Japaridze and A. A. Nersesyan, *JETP Lett.* **27**, 334 (1978).
- [23] T. Sakai and M. Takahashi, *Phys. Rev. B* **57**, 8091 (1998).
- [24] P.H. Hammar, D.H. Reich, C. Broholm and F. Trouw, *Phys. Rev. B* **57**, 7846 (1998) .
- [25] J.A. Hertz, *Phys. Rev. B* **14**, 1165 (1976); S. Sachdev, *Phys. Rev. B* **55**, 142 (1997), and refs. therein.